Journal of Environmental Protection and Ecology 21, No 2, 551–560 (2020)

Solid waste management

DISSOLUTION OF NICKEL IN BROMIDE-BASED SOLUTIONS USED AS LIXIVIANTS FOR WASTE PRINTED CIRCUIT BOARDS

S. VARVARA[a]*, S. A. DORNEANU[b], R. BOSTAN[a], M. POPA[a], AL. OKOS[c], G. DAMIAN[a], P. ILEA[b]

[a]*Department of Exact Sciences and Engineering, '1 Decembrie 1918' University of Alba Iulia, 15–17 Unirii Street, 510 009 Alba Iulia, Romania*
E-mail: *svarvara@uab.ro*
[b]*Department of Chemical Engineering, 'Babes-Bolyai' University, 11 Arany Janos Street, 400 028 Cluj-Napoca, Romania*
[c]*Physical and Chemical Analysis Department (RBRO/EQV-A), Parc Industrial Tetarom, Robert Bosch SRL, 3 Jucu Herghelie Street, 407 352 Cluj, Romania*

Abstract. The dissolution behaviour of nickel was investigated by electrochemical, XPS and SEM/EDX measurements in different Br/Br_2 systems that could be used as lixiviants in the hydrometallurgical route of metals recovery from waste printed circuit boards. Electrochemical impedance spectroscopy and polarisation measurements showed that Ni becomes passive in near neutral KBr solution and this fact hinders its dissolution. Instead, the dissolution of Ni was accelerated by decreasing the KBr solution's pH to 0.3 and even more in the presence of bromine, at a concentration of 0.01 M. Different electrical equivalent circuits have been proposed to broaden understanding the dissolution mechanism of nickel. XPS chemical assessment allowed the identification of the dissolution products formed on Ni surface after exposure to brominated electrolyte.

Keywords: electronic waste, printed circuit board, nickel dissolution, bromide/bromine solution.

AIMS AND BACKGROUND

The EU directive defines as 'waste electrical and electronic equipment' (WEEE) as the electrical or electronic equipment which is waste, including all components, sub-assemblies and consumables which are part of the product at the time of discarding[1,2].

The annual amount of E-wastes has reached 44.7 million metric t per year worldwide in 2016 and is forecasted to be 52.2 million t per year by 2021. In the European Union, approximately 10 million t of E-wastes are generated every year with an annual increase of 3 to 5%. The total value of all raw materials present in E-waste is estimated at approximately 55 billion Euros in 2016 (Ref. 3).

* For correspondence.

E-waste is a complex mixture of materials and components (>1000) such as metals (lead, mercury, arsenic, cadmium, selenium, hexavalent chromium), plastics, rubber, concrete and ceramics; with its composition depending largely on the type, manufacturer and age of the equipment[3–8].

The most hazardous part of the electronic waste is Printed Circuit Board (PCB) which can contain up to 40% metals, 30% ceramics and 30% organic materials/plastics[5,9]. The electronic components from waste PCBs (resistors, relays, capacitors, and integrated circuits), have a metal content of nearly 30% Cu;10–20% solder Pb; 1–5% Ni; 1–3% Fe; 4% Sn, 1% Zn; 0.05% Ag; 0.03% Au and 0.01% Pd. The purity of precious metals in PCBs is more than 10 times that of rich minerals[10,11].

Because of their hazardous content, and if not properly managed, can cause major environmental and health problems[12]. For instance, Ni intoxication causes dermatitis, skin allergies, pulmonary fibrosis, and cardiovascular and kidney disease[13], Pb affects blood systems, kidney, central and peripheral nervous systems and brain development of children, causing anemia, hypertension, risk for stroke and cardiovascular disease[14,15]; Cd can cause chronic renal failure, atherosclerosis and cardiovascular diseases[16]; poisoning with Zn causes cardiovascular, respiratory, renal, and hepatobiliary failure[14]; exposure to high levels of Cu can result in liver and kidney damage, anemia, and immunotoxicity[17]; Al affects the hematopoietic and nervous systems and the skeleton[14].

However, E-wastes are an important source of base and precious metals with high economic potential[3]. The existing processes for the recycling of Waste printed circuit boards (WPCBs) can be divided into mechanical (physical), pyrometallurgical, hydrometallurgical and bio-metallurgical process, as well as some hybrid processes[18,19].

Mechanical-physical separation steps, usually used in the pre-treatment process, included selectively dismantling, crushing and physical separation methods. The separation efficiency of physical PCB recycling systems is up to 99% (Ref. 20).

Pyrometallurgy can recycle some base metals such as Cu, Pb, Zn, etc., with high purity through smelting, refining process, but has some environmental limitations[10]. For instance, hydrometallurgical treatment of WPCBs has been found to be more efficient and environmentally friendly than physical separation and pyrometallurgical processes and could be preferred for the recovery of precious metals such as gold, silver and platinum. To transfer metals from solid materials to a solution for further recovery, leaching is an inevitable step in a hydrometallurgical process. The traditional hydrometallurgical approaches use mineral acids (HNO_3, H_2O_2–H_2SO_4) (Ref. 9), which can effectively leach many base metals from WPCBs but not precious metals. Since WPCBs recycling can only be profitable with substantial Au recovery, cyanide was used as lixiviants for precious metals. Cyanide is well known as a toxic chemical posing, but the advantages such as

cheaper reagent, less dosage, operating in an alkaline solution make it to be preferred in the gold mining industry[21].

The recent research focus has been very much on finding more benign and milder lixiviants and leach conditions. Thiosystem leaching (thiosulphate, thiourea and thiocyanate) and halide are mainly for precious metals leaching, while ammonia-ammonium is reported to leach base metals from WPCBs (Ref. 20). Although these lixiviants are low cost and environment-friendly, their disadvantage is related to their low chemical stability with low metal recovery.

In the present work, a fundamental study on the electrochemical dissolution behaviour of nickel was carried out using electrochemical, SEM and XPS measurements in different bromide-based electrolytes that could be used as lixiviants in hydrometallurgical route of metals recovery. This study is part of a complex research project aiming to elaborate an innovative and pollutants-free hydrometallurgical technology for metals recovery from WPCBs. The bromide/bromine (Br^-/Br_2) leaching system could be efficient for the dissolution of metals, due to its important characteristics such as fast leaching rate, non-toxicity and applicability over a wide range of pH values (from acidic to neutral). To the best of our knowledge, Br^-/Br_2 system was used before only for extraction of gold from gold ores[22].

EXPERIMENTAL

The dissolution tests were performed using a three-electrode cell; the working electrode was made from Ni metallic disk ($S = 0.28$ cm^2) embedded in epoxy resin (Buhler, EpoxycureTM), $Ag/AgCl/KCl_{sat}$ (Ref.) was used as reference electrode, while the counter-electrode was a twisted platinum wire ($\Phi = 0.5$ mm, $L = 10$ cm). The exposed metallic surface was prepared via an abrading procedure, using successive grade of silicon carbide paper grit (from 1200 up to 4000), washed thoroughly with distilled water and with ethanol.

Different bromide-based electrolytes were used as leaching systems, as follows: Sol. A – 2 M KBr (pH = 6); Sol. B – 2 M KBr + 0.5 M HBr (pH = 0.3) and Sol. C – 2 M KBr + 0.5 M HBr (pH = 0.3) + 0.01 M Br_2. All dissolution tests were performed in the electrolytes under non-stirred and naturally aerated conditions. The electrochemical measurements were carried out using a PAR model 2273 potentiostat. Potentiodynamic polarisation curves were recorded at constant sweep rate of 10 mV min^{-1}, in a wide potential range of ± 250 mV versus OCP from the cathodic to the anodic direction. The impedance spectra were recorded at OCP in the frequency range of 10 kHz – 10 mHz at 5 points per hertz decade, using an AC voltage amplitude of ± 10 mV.

XPS and SEM/EDX data were collected using a custom built Thermofisher ESCALAB 250 Xi XPS spectrometer equipped with a scanning electron microscope and an X-ray detector for the acquisition of EDX data. The XPS spectra

were acquired using the Al Kα radiation (1486.6 eV). The data were collected from circular surface with a radius of 650 μm. The XPS spectra were recorded and fitted using the Avantage software.

RESULTS AND DISCUSSION

Electrochemical measurements. In order to obtain information on the electrochemical processes taking place at Ni interface in different bromide-based electrolytes, potentiodynamic polarisation measurements and electrochemical impedance spectroscopy (EIS) were carried out. The measurements were conducted at the open-circuit potentials and the obtained polarisation curves and Nyquist plots are depicted in Fig. 1.

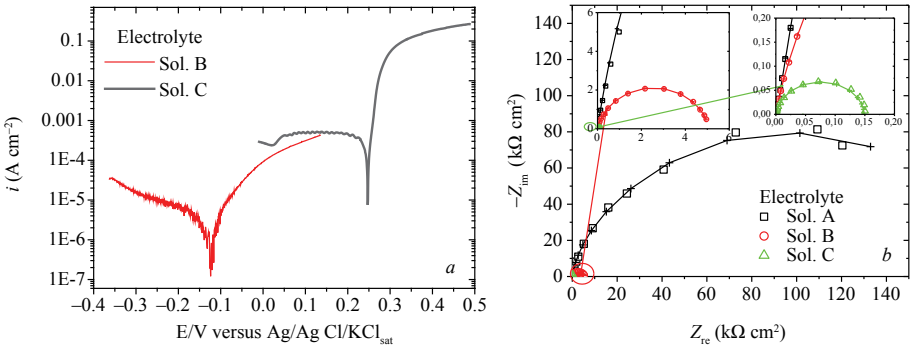

Fig. 1. Polarisation curves (*a*) and impedance diagrams (*b*) for nickel dissolution in different bromide-based electrolytes

It should be mentioned that the Ni dissolution could not be achieved in the near neutral KBr solution (pH 6) due to strong passivation of the metal, but it was accomplished to a low extent in more acidic KBr electrolyte (pH 0.3). Instead, the addition of Br_2 significantly enhances both the active dissolution of Ni and oxygen reduction, as proved by the significant displacement of the anodic and cathodic branches of the polarisation curves toward higher current densities values. A shift of the corrosion potential towards more positive values could be also noticed in the presence of Br_2, while the cathodic process appears to be under diffusion control.

The electrochemical parameters derived from the polarisation curves, such as corrosion potential (E_{corr}), cathodic and anodic Tafel slopes (β_c and β_a), corrosion current density (i_{corr}) were calculated according to the Tafel equation (1) and are summarised in Table 1.

$$i = i_0 \left(\exp \frac{\beta_a z F (E - E_{corr})}{RT} - \exp \left(- \frac{\beta_c z F (E - E_{corr})}{RT} \right) \right), \quad (1)$$

where i_{corr} is the corrosion current density; E – the electrode potential; E_{corr} – the corrosion potential; z – the number of electrons transferred; F – the Faraday constant; R – the universal gas constant; T – the absolute temperature; β_a and β_c – the anodic and cathodic Tafel coefficients, respectively.

The dissolution rate of nickel (mm/h) was also calculated based on the following equation:

$$v_{diss} = 3.268 \times 10^3 (E_w/\rho) (I_{corr}/S), \quad (2)$$

where E_w is the equivalent weight of the sample (g); S – the sample area (cm^2); ρ – the sample density (g/cm^3), and I_{corr} – the current density (A).

Table 1. Electrochemical parameters and dissolution rates for Ni in different solutions

Solution	E_{corr} (mV vs. Ref.)	i_{corr} (μA cm^{-2})	$\lvert\beta_c\rvert$ (mV/dec)	$\lvert\beta_a\rvert$ (mV/dec)	v_{diss} (mm/h)
B	–125.36	1.6	110.8	51.9	0.002
C	+ 247.50	141.0	13.3	13.2	0.170

Regarding the electrochemical impedance diagrams, it could be observed from Fig. 1*b* that the value of the impedance corresponding to Ni dissolution in sol. A is significantly higher than the value of the impedance obtained in strong acidic solutions (sol. B and sol. C). This behaviour confirms the strong passivation of Ni surface in near neutral KBr (pH 6) solution, which hinders its dissolution. Instead, the significant decrease of the impedance magnitude observed in sol. B as compared to sol. A and, even more in the presence of Br_2 (sol. C), is consistent with an increased dissolution rate of Ni in strong acidic electrolytes. The appearance of an inductive behaviour in the impedance diagram obtained in sol. C confirms that the dissolution mechanism of Ni is different in the presence of Br_2, as compared to its absence, in agreement with the polarisation measurements results.

EIS results were further analysed by numerical simulation, using different equivalent electrical circuits that allows the estimation of the *R*–*Q* parameters corresponding to the electrochemical systems under investigation. The equivalent electrical circuits used for experimental EIS data simulation are illustrated in Fig. 2 and the calculated *R*–*Q* parameters are presented in Table 2.

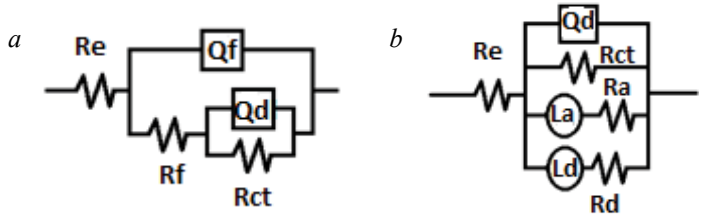

Fig. 2. Equivalent electrical circuits used for EIS data simulation

The impedance corresponding to Ni dissolution in sol. A and sol. B could be suitably represented using two-time constants under capacitive relaxation, according to the electrical circuit from Fig. 2*a*. In this circuit, R_e represents the solution resistance; R_f–Q_f couple is ascribed to the resistance and capacitance of a passive oxide layer (i.e. NiO and/or $Ni(OH)_2$) formed on Ni surface and R_{ct}–Q_d parameters correspond to charge transfer resistance and double layer capacitance.

An inductive contribution at intermediate and low frequencies is clearly visible in the EIS spectra of Ni obtained in the presence of 0.01 M Br_2. Several models of equivalent circuits were attempted to fit these experimental data. The best agreement between experiment and fitting results was obtained using the equivalent circuit from Fig. 2*b*. It contains one capacitive loop attributed to the charge transfer reaction (R_{ct}–Q_d) and two *R*–*L* couples. The first indictive couple (R_a–L_a) could be ascribed to the coverage relaxation of some intermediates, i.e. $NiOH_{ads}^+$ formed in Br_2-containing electrolytes. The presence of different Ni oxide states on the surface was identified by XPS. The second inductive couple (R_d–L_d) might be attributed to the re-dissolution of the Ni species formed on surface, explaining the high dissolution rate of Ni in the presence of bromine.

In Fig. 1*b* the lines marked with cross represents the simulated data while the symbols are associated to the measured results. In all investigated electrolytes, the used equivalent circuits well reproduce the experimental impedance data, as can be readily seen in Fig. 1*b*, where a good overlap between the measured and calculated data was obtained. Table 2 presents the electrochemical parameters obtained by fitting the experimental data to the equivalent electrical circuits.

Table 2. Values of *R*–*Q* parameters obtained for Ni dissolution in bromide-based electrolytes

Sol.	R_e (Ω cm^2)	R_f (kΩ cm^2)	Q_f (μFs^{n-1}/cm^2)	n_f	R_{ct} (kΩ cm^2)	Q_d (μFs^{n-1}/cm^2)	n_d	R_a (Ω cm^2)	L_a (H cm^2)	R_d (Ω cm^2)	L_d (H cm^2)
A		131.7	35.5	0.92	54.3	73.3	0.98	–	–	–	–
B	0.51	1.2	22.7	0.92	3.9	14.9	0.77	–	–	–	–
C	0.56	–	–	–	0.15	16.8	–	264.4	60.04	89.0	302.4

n_f and n_d are parameters related to the depressed features of the experimental EIS.

It is well-known that a large charge transfer resistance (R_{ct}) is associated with a less corroding system[23]. As shown in Table 2, the charge transfer resistance, R_{ct} values decrease as the electrolyte' pH becomes acidic and this effect is highly enhanced by the addition of Br_2. Thus, the calculated R_{ct} value is almost 14 times lower in sol. B as compared to sol. A, which proves that the Ni dissolution process is highly favoured by pH decreasing. This agrees with the variation of the film resistance, R_f value, which is more than 107 times smaller in sol. B, as compared to sol. A, confirming that the passivation of Ni is strongly inhibited in KBr (pH 0.3)

solution. However, the lowest value of R_{ct} was obtained in sol. C; it is almost 361 and 26 times smaller in sol. C, as compared to sol. A and sol. B, respectively. These results advice for an increased dissolution rate of Ni in Br_2-containing electrolyte, in good agreement with the polarisation measurements.

XPS and SEM/EDX measurements. XPS and SEM/EDX analyses were performed on Ni surface after exposure for 48 h to sol. C. The regions analysed by EDX and XPS have comparable areas (600 × 600 μm for EDX, a circle with a 650 μm diameter for XPS).

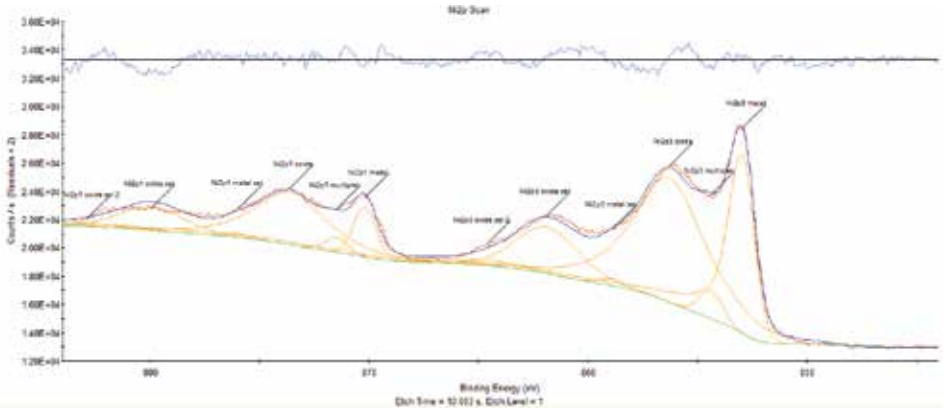

Fig. 3. Ni 2*p* narrow scan fit after 10 s of etching, when all components become clearly visible

The Ni 2*p* narrow (Fig. 3) scans present complicated spectra in which at least two different contributions can be distinguished, i.e. a metallic Ni phase presenting multiplet splitting and satellite features and at least one oxidised Ni^{2+} phase which also presents satellite features. Two sets of satellite peaks associated with the oxidised phase appear to be required in order to obtain a featureless residue. This could indicate the presence on the surface of the sample of more complicated Ni compounds.

Table 3 gives the Binding energy (BE) values for the main peaks of the two Ni phases observed on the surface. The Full width at half maximum (FWHM) parameter of the main Ni $2p_{3/2}$ peaks is also shown in Table 3. The data were acquired in constant analyser energy mode with a pass energy of 30 eV. In this configuration the instrumental broadening is 1 eV. It can be observed from Table 3 that the width of oxide phase Ni $2p_{3/2}$ peak is more than 3.5 times the instrumental broadening. This also indicates the presence of more complicated chemical phases on the surface of the sample.

The value of BE for the oxide component seems to indicate the formation of $Ni(OH)_2$. The observed Ni to O atomic ratio averaged on three different acquisition regions is Ni:O = 63.22:36.77 = 1.7:1. The Ni contribution is calculated using

only the area of the Ni $2p_{3/2}$ oxide peak and neglecting the area of the satellite peaks. This method is simplifying the calculations but is underestimating the Ni concentration. However, even under this approximation excess, Ni is observed. This result further indicates the presence of a mixture of different Ni oxide states on the metallic surface.

Table 3. Binding energies of the observed Ni species

Peak	State	Observed BE (eV)	Corrected BE (–0.5 eV)	FWHM (eV) at 30 eV pass energy	Literature BE (eV)	Possible compound
Ni $2p_{3/2}$ metal	0	853.0	852.5	1.36	852.6 (Ref. 24)	Ni
Ni $2p_{3/2}$ oxide	2+	856.3	855.8	3.68	853.7 (Ref. 24)	NiO
					854.9 (Ref. 24)	$Ni(OH)_2$
					855.7 (Ref. 25)	

Figure 4 shows SEM-EDX maps containing the distribution of Ni, Br and K on the Ni surface. It can be observed that the regions which contain Br also present a high concentration of K. EDX mapping shows Br is not distributed homogeneously on the surface of the sample whereas Ni is.

Fig. 4. SEM-EDX maps showing the regions containing Ni (*a*), Br (*b*) and K (*c*)

CONCLUSIONS

In the present paper, the dissolution behaviour of nickel in different bromide-based electrolytes was investigated using electrochemical and surface characterisation techniques.

Potentiodynamic polarisation and electrochemical impedance spectroscopy measurements showed that nickel becomes passive in near neutral KBr solution (pH 6), which hinders its dissolution. In highly acidic KBr solution (pH 0.3), the dissolution rate of nickel is enhanced, and this effect is more pronounced in the presence of bromine. EIS measurements allowed explaining the nickel dissolution mechanism in the investigated electrolytes, while XPS chemical assessment

confirmed the presence of NiO and $Ni(OH)_2$ on the metallic surface after exposure to brominated electrolyte.

The increased dissolution rate of nickel obtained in the bromine-containing solution strongly recommend its use as an effective lixiviant in the hydrometallurgical route of metals recovery.

Acknowledgements. This work was supported by a grant of the Romanian Ministry of Research and Innovation, CCCDI-UEFISCDI, project number PN-III-P1-1.2-PCCDI-2017-0652/84PCCDI/ 2018, within PNCDI III.

REFERENCES

1. Directive 2012/19/EU of the European Parliament and of the Council of 4 July 2012 on WEEE. 2012.
2. E. ZEBEK, M. SZWEJKOWSKA, M. RACZKOWSKI: Legal and Organisational Solutions of Municipal Waste Management in Poland in Compliance with Waste Directive 2008/98/EC. J Environ Prot Ecol, **16** (2), 652 (2015).
3. A. IŞILDAR, E. R. RENE, E. D. VAN HULLEBUSCH, P. N.L. LENS: Electronic Waste as a Secondary Source of Critical Metals: Management and Recovery Technologies. Resour Conserv Recycl, **135**, 296 (2018).
4. C. P. BALDÉ, V. FORTI, V. GRAY, R. KUEHR, P. STEGMANN: The Global E-waste Monitor. United Nations University (UNU), International Telecommunication Union (ITU) & International Solid Waste Association (ISWA), Bonn, Germany, 2017.
5. S. PINHO, M. FERREIRA, M. F. ALMEIDA: A Wet Dismantling Process for the Recycling of Computer Printed Circuit Boards. Resour Conserv Recycl, **132**, 71 (2018).
6. E. KARWOWSKA, D. ANDRZEJEWSKA-MORZUCH, M. LEBKOWSKA et al.: Bioleaching of Metals from Printed Circuit Boards Supported with Surfactant-producing Bacteria. J Hazard Mater, **264**, 203 (2014).
7. Y. JAE-MIN, J. JINKI, Y. KYOUNGKEUN, L. JAE-CHUN, K. WONBAEK: Enrichment of the Metallic Components from Waste Printed Circuit Boards by a Mechanical Separation Process Using a Stamp mill. Waste Manage, **29**, 1132 (2009).
8. H. CHEN, B. YANG, X. CHEN: Identification and Characterization of Four Strains of Acidithiobacillus ferrooxidans Isolated from Different Sites in China. Microbiol Res, **164**, 613 (2009).
9. K. MANOJ, L. JAE-CHUN, K. MIN-SEUK, J. JINKI, Y. KYOUNGKEUN: Leaching of Metals from Waste Printed Circuit Boards (WPCBs) using Sulfuric and Nitric Acids. Environ Eng Manag J, **13** (10), 2601 (2014).
10. K. MUAMMER: Recovery of Metals and Non-metals from Electronic Waste by Physical and Chemical Recycling Processes. Waste Manage, **57**, 64 (2016).
11. Y. ZHOU, K. QIU: A New Technology for Recycling Materials from Waste Printed Circuit Boards. J Hazard Mater, **175**, 823 (2010).
12. B. DEBNATH, P. ROYCHOWDHURY, R. KUNDU: Electronic Components (EC) Reuse and Recycling – a New Approach towards WEEE Management. Procedia Environ Sci, **35**, 356 (2016).
13. A. DUDA-CHODAK, U. BŁASZCZYK: The Impact of Nickel on Human Health. J Elem, **13**, 685 (2008).
14. J. RODRIGUEZ, P. M. MANDALUNIS: A Review of Metal Exposure and Its Effects on Bone Health. J Toxicol, 1 (2018).
15. N. VELICKOVA: Environmental Impact of Heavy Metals on the Blood Cells in Professionally Exposed Workers. J Environ Prot Ecol, **18**, 363 (2017).

16. N. N. DONGRE, A. N. SURYAKAR, A. J. PATIL, I. A. HUNDEKARI, B. B. DEVARNAVADAGI: Biochemical Effects of Lead Exposure on Battery Manufacture Workers with Reference to Blood Pressure, Calcium Metabolism and Bone Mineral Density. Indian J Clin Biochem, **28**, 65 (2013).
17. B. MESSNER, D. BERNHARD: Cadmium and Cardiovascular Diseases: Cell Biology, Pathophysiology, and Epidemiological Relevance. Biometals, **23**, 811 (2010).
18. A. AKCI, C. ERUST, C. S. GAHAN, M. OZGUN, M. SAHIN, A. TUNCUK: Precious Metal Recovery from Waste Printed Circuit Boards Using Cyanide and Non-cyanide Lixiviants – a Review. Waste Manage, **45**, 258 (2015).
19. R. JUJUN, Z. XINGJIONG, Q. YIMING, H. JIAN: A New Strain for Recovering Precious Metals from Waste Printed Circuit Boards. Waste Manage, **34**, 901 (2014).
20. Z. YANHUA, L. SHILI, X. HENGHUA, Z. XIANLAI, L. JINHUI: Current Status on Leaching Precious Metals from Waste Printed Circuit Boards. Procedia Environ Sci, **16**, 560 (2012).
21. Agency for Toxic Substances and Disease Registry (ATSDR): Toxicological Profile for Copper, Department of Health and Human Services, Public Health Service, Atlanta, USA, 2004.
22. R. SOUSA, A. FUTURO, A. FIÚZA, M.C. VILA, M.L. DINIS: Bromine Leaching as an Alternative Method for Gold Dissolution. Miner Eng, **118**, 16 (2018).
23. X. LI, S. DENG, H. FU: Inhibition of the Corrosion of Steel in HCl, H_2SO_4 Solutions by Bamboo Leaf Extract. Corr Sci, **62**, 163, (2012).
24. M. C. BIESINGER, B. P. PAYNE, L. W. M. LAU, A. GERSON, R. St. C. SMART: X-ray Photoelectron Spectroscopic Chemical State Quantification of Mixed Nickel Metal, Oxide and Hydroxide Systems. Surf Interface Anal, **41**, 324 (2009).
25. A. M. VENEZIA, R. BERTONCELLO, G. DEGANELLO: X-ray Photoelectron Spectroscopy Investigation of Pumice-supported Nickel Catalysts. Surf Interface Anal, **23**, 239 (1995).

Received 23 January 2020
Revised 12 February 2020